[7] M. L. Hilton, "Wavelet and wavelet packet compression of electrocardiograms," *IEEE Trans. Biomed. Eng.*, vol. 44, no. 5, pp. 394–402, May 1997.
[8] A. Djohan, T. Q. Nguyen, and W. J. Tompkins, "ECG compression using discrete symmetric wavelet transform," in *Proc. IEEE Int. Conf. Engineering in Medicine and Biology Society*, Sep. 20-23, 1995, vol. 1, pp. 167–168.
[9] S. G. Miaou, H. L. Yen, and C. L. Lin, "Wavelet-based ECG compression using dynamic vector quantization with tree codevectors in single codebook," *IEEE Trans. Biomed. Eng.*, vol. 49, no. 3, pp. 671–680, Mar. 2002.
[10] S. G. Miaou and S. N. Chao, "Wavelet-based lossy-to-lossless ECG compression in a unified vector quantization framework," *IEEE Trans. Biomed. Eng.*, vol. 52, no. 3, pp. 539–543, Mar. 2005.
[11] M. Blanco-Velasco, F. Cruz-Roldan, J. I. Godino-Llorente, and K. E. Barner, "ECG compression with retrieved quality guaranteed," *Electron. Lett., 11th*, vol. 40, no. 23, pp. 1466–1467, Nov. 2004.
[12] M. Vishwanath, "The recursive pyramid algorithm for the discrete wavelet transform," *IEEE Trans. Signal Process.*, vol. 42, no. 3, pp. 673–677, Mar. 1994.
[13] K. C. Hung, Y. J. Huang, F. C. Hsieh, and J. C. Wang, "An AOCA-based VLSI architecture for non-recursive 2D discrete periodized wavelet transform," in *Proc. 14th Int. Conf. Digital Signal Processing*, Santorini, Greece, Jul. 1-3, 2002, vol. 1, pp. 273–276.
[14] C. F. Tsai, H. S. Wang, and K. C. Hung, "A high efficient nonrecursive discrete periodized wavelet transform for extracting the transformed coefficients of coarser resolution levels," in *Proc. 2004 IEEE Asia-Pacific Conf. Circuits And Systems*, Dec. 6-9, , pp. 661–664.
[15] G. B. Moody and R. G. Mark, "The impact of the MIT/BIH arrhythmia database," *IEEE Eng. Med. Biol. Mag.*, vol. 20, no. 3, pp. 45–50, May/Jun. 2001.
[16] K. C. Hung, Y. S. Hung, and Y. J. Huang, "A nonseparable VLSI architecture for 2D discrete periodized wavelet transform," *IEEE Trans. VLSI Syst.*, vol. 9, no. 5, pp. 565–576, Oct. 2001.
[17] W. B. Pennebaker and J. L. Mitchell, *JPEG Still Image Data Compression Standard*. New York: Van Nostrand Reinhold, 1993.

Canonical Correlation Analysis Applied to Remove Muscle Artifacts From the Electroencephalogram

Wim De Clercq*, Anneleen Vergult, Bart Vanrumste, Wim Van Paesschen, and Sabine Van Huffel

***Abstract*—The electroencephalogram (EEG) is often contaminated by muscle artifacts. In this paper, a new method for muscle artifact removal in EEG is presented, based on canonical correlation analysis (CCA) as a blind source separation (BSS) technique. This method is demonstrated on a synthetic data set. The method outperformed a low-pass filter with different cutoff frequencies and an independent component analysis (ICA)-based technique for muscle artifact removal. In addition, the method is applied on a real ictal EEG recording contaminated with muscle artifacts. The proposed method removed successfully the muscle artifact without altering the recorded underlying ictal activity.**

***Index Terms*—Blind source separation, canonical correlation analysis, EEG, muscle artifact removal.**

I. Introduction

The electroencephalogram (EEG) is frequently contaminated by electrophysiological potentials associated with muscle contraction due to biting, chewing and frowning. These muscle artifacts obscure the EEG and complicate the interpretation of the EEG or even make the interpretation unfeasible [1].

Low-pass filters are commonly used to remove muscle artifact. However, as the frequency spectrum of muscle artifacts overlaps with that of interesting brain signals [2], frequency filters not only suppress muscle artifacts but also valuable information. A more recently explored approach is independent component analysis (ICA) which separates the EEG into statistical independent components. However, crosstalk of brain and muscle activity can be observed [3], [4].

In this paper, a new method for muscle artifact removal in EEG is presented, based on the statistical Canonical Correlation Analysis (CCA) [5] applied as a blind source separation (BSS) technique [6], further referred to as BSS-CCA. To solve the BSS problem, BSS-CCA assumes mutually uncorrelated sources which are maximally autocorrelated [6]. BSS-CCA was applied for the separation of muscle and brain activity sources because of the relative low autocorrelation of muscle artifacts in comparison with brain activity. The performance of the method was tested on synthetic data and compared with a low-pass filter with different cutoff frequencies and an ICA-based technique for

Manuscript received March 25, 2005; revised April 3, 2006. This work was supported in part by the the Research Council KUL: AMBioRICS, several Ph.D./postdoc and fellow grants; Flemisch governement: FWO: Ph.D./postdoc grants, projects, G.0360.05 (EEG signal processing for epileptic seizure analysis), G.0312.06 (tensor-based methods for spectral analysis), research communities (ICCoS, ANMMM); IWT: Ph.D. grants; Belgian Federal Science Policy Office IUAP P5/22 (Dynamical Systems and Control: Computation, Identification and Modelling); EU: BIOPATTERN (FP6-2002-IST 508803), and ETUMOUR (FP6-2002-LIFESCIHEALTH 503094). *Asterisk indicates corresponding author.*

*W. De Clercq is with the Department of Electrical Engineering ESAT-SCD(SISTA), Katholieke Universiteit Leuven, 3001 Leuven, Belgium (e-mail: wim.declercq@lrd.kuleuven.be).

A. Vergult, B. Vanrumste, and S. Van Huffel are with the Department of Electrical Engineering ESAT-SCD(SISTA), Katholieke Universiteit Leuven, 3001 Leuven, Belgium.

W. Van Paesschen is with the Department of Neurology, University Hospital Gasthuisberg, 3000 Leuven, Belgium.

Digital Object Identifier 10.1109/TBME.2006.879459

0018-9294/$20.00 © 2006 IEEE

muscle artifact removal. Furthermore, the method was applied on a real ictal EEG recording contaminated with muscle artifacts.

II. Blind Source Separation by Canonical Correlation Analysis for Artifact Removal

In the BSS problem, the observed time course $\mathbf{X}(t) = [\mathbf{x}_1(t), \mathbf{x}_2(t), \ldots, \mathbf{x}_K(t)]^T$, with $t = 1, \ldots, N$, with N the number of samples and K the number of sensors, is the result of an unknown mixture of a set of unknown source signals $\mathbf{S}(t) = [\mathbf{s}_1(t), \mathbf{s}_2(t), \ldots, \mathbf{s}_K(t)]^T$. The mixing is assumed to be linear, thus reducing the mixing to a matrix multiplication

$$\mathbf{X}(t) = \mathbf{A}\mathbf{S}(t) \tag{1}$$

where $\mathbf{A}$ is the unknown mixing matrix. The goal is to estimate the mixing matrix and recover the original source signals $\mathbf{S}(t)$. This is carried out by introducing the de-mixing matrix $\mathbf{W}$ such that

$$\mathbf{Z}(t) = \mathbf{W}\mathbf{X}(t) \tag{2}$$

approximates the unknown source signals in $\mathbf{S}(t)$, by a scaling factor. Ideally, $\mathbf{W}$ is the inverse of the unknown mixing matrix $\mathbf{A}$, up to a scaling and permutation. Unless there are extra constraints imposed, it is in general impossible to solve this source separation problem. CCA solves the problem by forcing the sources to be maximally autocorrelated and mutually uncorrelated, furthermore the mixing matrix is assumed to be square [6], [7].

Let $\mathbf{X}(t)$ be the observed data matrix with K mixtures and N samples, and let $\mathbf{Y}(t)$ be a temporally delayed version of the original data matrix $\mathbf{Y}(t) = \mathbf{X}(t-1)$. When the mean of each row from the data matrices $\mathbf{X}(t)$ and $\mathbf{Y}(t)$ is removed, CCA obtains two sets of basis vectors, one for $\mathbf{X}$ and the other for $\mathbf{Y}$, such that the correlations between the projections of the variables onto these basis vectors are mutually maximized. Consider the linear combinations of the components in $\mathbf{X}$ and $\mathbf{Y}$, called the variates

$$\begin{aligned} \mathbf{u} &= w_{x_1}\mathbf{x}_1 + \ldots + w_{x_K}\mathbf{x}_K = \mathbf{w}_\mathbf{x}^T\mathbf{X} \\ \mathbf{v} &= w_{y_1}\mathbf{y}_1 + \ldots + w_{y_K}\mathbf{y}_K = \mathbf{w}_\mathbf{y}^T\mathbf{Y}. \end{aligned} \tag{3}$$

CCA finds the weight vectors $\mathbf{w_x} = [w_{x_1}, \ldots, w_{x_K}]^T$ and $\mathbf{w_y} = [w_{y_1}, \ldots, w_{y_K}]^T$ that maximize the correlation ρ between the variates $\mathbf{u}$ and $\mathbf{v}$ by solving the following maximization problem:

$$\begin{aligned} &\max_{\mathbf{w_x}, \mathbf{w_y}} \rho(\mathbf{u}, \mathbf{v}) \\ &= \frac{E[\mathbf{uv}]}{\sqrt{E[\mathbf{u}^2]E[\mathbf{v}^2]}} \\ &= \frac{E\left[\left(\mathbf{w}_\mathbf{x}^T\mathbf{X}\right)\left(\mathbf{w}_\mathbf{y}^T\mathbf{Y}\right)\right]}{\sqrt{E\left[\left(\mathbf{w}_\mathbf{x}^T\mathbf{X}\right)\left(\mathbf{w}_\mathbf{x}^T\mathbf{X}\right)\right] E\left[\left(\mathbf{w}_\mathbf{y}^T\mathbf{Y}\right)\left(\mathbf{w}_\mathbf{y}^T\mathbf{Y}\right)\right]}} \\ &= \frac{\mathbf{w}_\mathbf{x}^T\mathbf{C_{xy}}\mathbf{w_y}}{\sqrt{\left(\mathbf{w}_\mathbf{x}^T\mathbf{C_{xx}}\mathbf{w_x}\right)\left(\mathbf{w}_\mathbf{y}^T\mathbf{C_{yy}}\mathbf{w_y}\right)}} \end{aligned} \tag{4}$$

with $\mathbf{C_{xx}}$ and $\mathbf{C_{yy}}$ the autocovariance matrices of $\mathbf{X}$ and $\mathbf{Y}$, respectively, and $\mathbf{C_{xy}}$ the crosscovariance matrix of $\mathbf{X}$ and $\mathbf{Y}$. The maximization problem can be solved by setting the derivatives of (4) with respect to $\mathbf{w_x}$ and $\mathbf{w_y}$ to zero, which after some manipulation results in the following two eigenvalue problems [8], [9]

$$\begin{cases} \mathbf{C}_{xx}^{-1}\mathbf{C}_{xy}\mathbf{C}_{yy}^{-1}\mathbf{C}_{yx}\hat{\mathbf{w}}_\mathbf{x} = \rho^2\hat{\mathbf{w}}_\mathbf{x} \\ \mathbf{C}_{yy}^{-1}\mathbf{C}_{yx}\mathbf{C}_{xx}^{-1}\mathbf{C}_{xy}\hat{\mathbf{w}}_\mathbf{y} = \rho^2\hat{\mathbf{w}}_\mathbf{y} \end{cases} \tag{5}$$

with the canonical correlation coefficient ρ as the square root of the eigenvalue, and $\mathbf{w_x}$ and $\mathbf{w_y}$ as eigenvectors. Once the pair $\mathbf{w_x}$ and $\mathbf{w_y}$ that maximizes the correlation between $\mathbf{w}_\mathbf{x}^T\mathbf{X}$ and $\mathbf{w}_\mathbf{y}^T\mathbf{Y}$ is found, a second pair of weight vectors $\tilde{\mathbf{w}}_\mathbf{x}$ and $\tilde{\mathbf{w}}_\mathbf{y}$ can be obtained that generates variates ($\tilde{\mathbf{w}}_\mathbf{x}^T\mathbf{X}$ and $\tilde{\mathbf{w}}_\mathbf{y}^T\mathbf{Y}$) which are maximally correlated with each other and uncorrelated with the variates of the first pair. The next pair(s) of weight vectors can again be found by maximizing (4), restricted to the fact that the variates are uncorrelated to all previously found variates. Of course, because $\mathbf{X}$ and $\mathbf{Y}$ contain almost the same data, $\mathbf{w_x}$ and $\mathbf{w_y}$ will essentially also contain the same data. Therefore, it is sufficient to solve (5) only for $\hat{\mathbf{w}}_\mathbf{x}$. The first variates constructed by CCA, $\mathbf{u}_1(t) = \mathbf{w}_\mathbf{x}^T\mathbf{X}(t)$ and $\mathbf{v}_1(t) = \mathbf{w}_\mathbf{y}^T\mathbf{Y}(t)$ are, thus, maximally correlated with each other, and because $\mathbf{Y}(t)$ is a one sample delayed version of $\mathbf{X}(t)$, these variates are related to each other as

$$\mathbf{v}_1(t) = \mathbf{w}_\mathbf{y}^T\mathbf{Y}(t) = \mathbf{w}_\mathbf{x}^T\mathbf{X}(t-1) = \mathbf{u}_1(t-1). \tag{6}$$

Consequently, of all linear transformations of the original time courses in $\mathbf{X}(t)$, $\mathbf{w_x}$ gives the transformation that yields the time course $\mathbf{u}_1(t)$ that has maximal autocorrelation (at lag one). The next pair(s) of variates yield the time course(s) $\mathbf{u}_i(t)$ having maximal autocorrelation among all possible linear combinations of the measured time courses which are uncorrelated with the previously obtained time courses. As a consequence, by putting the obtained variates equal to the sources: $\mathbf{u}_i(t) = \mathbf{z}_i(t)$, BSS-CCA finds sources which are uncorrelated with each other, maximally autocorrelated and ordered by decreasing autocorrelation index ρ_i.

When BSS-CCA is applied to the EEG and the sources, or components, contributing to the EEG are derived, the muscle artifact can be removed by setting the columns representing the activations of the artifactual sources equal to zero in the reconstruction $\mathbf{X}_{\text{clean}}(t)$:

$$\mathbf{X}_{\text{clean}}(t) = \mathbf{A}_{\text{clean}}\mathbf{Z}(t) \tag{7}$$

with $\mathbf{Z}(t)$ the sources obtained by BSS-CCA, and $\mathbf{A}_{\text{clean}}$ the mixing matrix with the columns representing activations of the muscle artifactual sources, set to zero. Due to the broad frequency spectrum of EMG contamination in scalp EEG recordings [2], muscle artifacts yield more properties of temporally white noise, thus having a low autocorrelation. Therefore, we expect the muscle artifacts to be present in the lowest autocorrelated BSS-CCA sources.

III. Simulation Study

The aim of the simulation study was to evaluate the performance of the proposed method in removing muscle artifacts. Several simulations with different signal-to-noise ratios (SNRs) were performed.

A. Brain Activity

An EEG epoch of 10 s containing mainly alpha (8–13 Hz) activity was selected as underlying brain signal. In the selected EEG, no muscle

artifact was present according to the visual inspection of an experienced neurophysiologist. The data was collected from 21 scalp electrodes placed according to the International 10–20 System [10] with additional electrodes $T1$ and $T2$ on the temporal region. The sampling frequency was 250 Hz and an average reference was used. The EEG epoch was stored in a 21×2500 dimensional matrix $\mathbf{B}$.

B. Muscle Activity

To obtain only muscle activity, necessary for the simulation study, it is not sufficient to select muscle artifacts in the EEG as these events will not only contain muscle activity but also activity from the brain. To remove the EEG activity we used ICA (SOBI) [11] to decompose these events. Note that for a large number of events, which were visually inspected by an experienced neurophysiologist, no clear separation was established. However, in some cases a component containing pure EMG activity could be observed (in addition to components containing both EMG and ongoing EEG activity), and was selected together with the corresponding field distribution. This procedure was repeated for three different 10 s EEG epochs recordings from three different subjects. Each individual component was reconstructed into a conventional EEG format by using the corresponding field distribution. Finally, all three reconstructions were summed and the resulting average referenced signal containing all three independent muscle activities was stored in a 21×2500 dimensional matrix $\mathbf{M}$.

C. Data and Measures to Test the Performance

In the simulation study, the average referenced muscle artifact signal $\mathbf{M}$ was superimposed on the average referenced signal $\mathbf{B}$ containing only brain activity

$$\mathbf{X}(\lambda) = \mathbf{B} + \lambda \cdot \mathbf{M} \tag{8}$$

with λ representing the contribution of muscle activity. The Root Mean Squared (RMS) value of the brain signal is then equal to

$$\mathrm{RMS}(\mathbf{B}) = \sqrt{\frac{1}{K \cdot N} \sum_{k=1}^{K} \sum_{n=1}^{N} \mathbf{B}^2(k,n)} \tag{9}$$

with N equal to the number of time samples and K equal to the number of EEG channels. An important measure is the SNR which is defined as follows:

$$\mathrm{SNR} = \frac{\mathrm{RMS}(\mathbf{B})}{\mathrm{RMS}(\lambda \cdot \mathbf{M})}. \tag{10}$$

Changing the λ parameter alters the SNR of the simulated signal. Several simulations with different SNRs were performed. The performance is expressed in terms of the relative root-mean-squared error (RRMSE)

$$\mathrm{RRMSE} = \frac{\mathrm{RMS}(\mathbf{B} - \hat{\mathbf{B}})}{\mathrm{RMS}(\mathbf{B})} \tag{11}$$

where $\hat{\mathbf{B}}$ is the signal after muscle artifact removal.

D. Methods for Comparison

For comparison, the proposed technique is compared with other commonly used techniques for muscle artifact removal as follows.

- Low-pass filter: a low-pass Butterworth filter of order 8 was used with four different cutoff frequencies equal to 10, 15, 20, and 30 Hz.

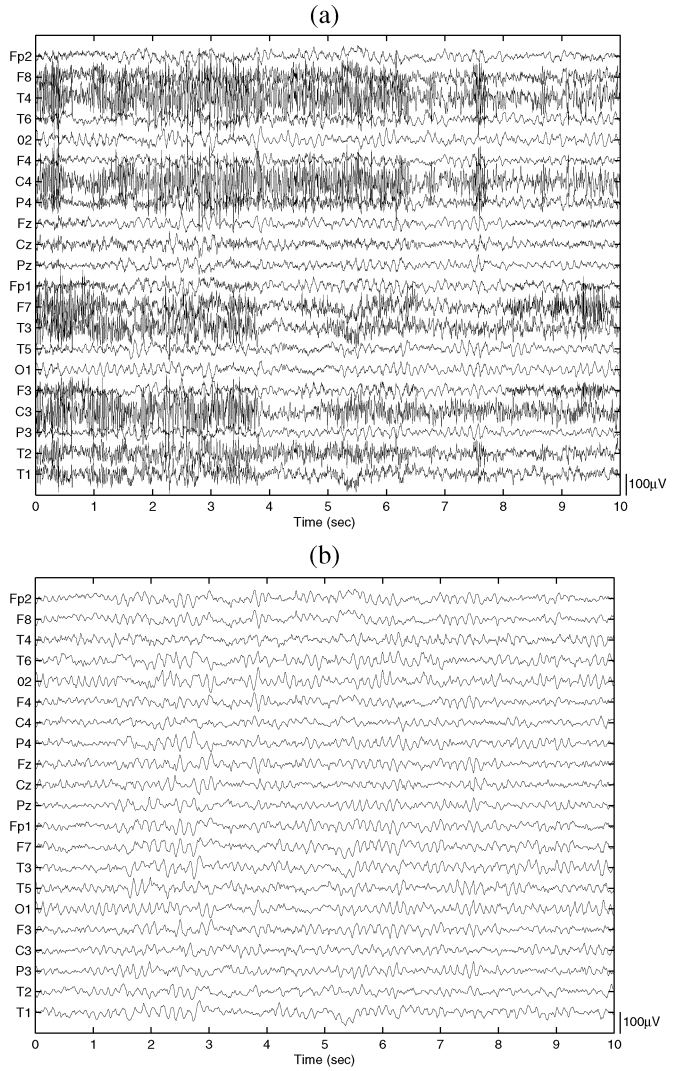

Fig. 1. (a) Simulation matrix $\mathbf{X}$ containing: alpha activity $\mathbf{B}$ and superimposed muscle activity $\mathbf{M}$ with $\mathrm{SNR} = 0.65$; (b) BSS-CCA processed data.

- ICA: as it is not in the scope of this paper to compare all different ICA algorithms, we limited ourself to the Joint Approximate Diagonalization of Eigen-matrices (JADE) algorithm [12], previously used in two studies for muscle artifact removal in scalp EEG recordings [4], [13]. The selection of the ICA(JADE) components accounting for the muscle artifact was based on visual inspection and the signal was reconstructed, excluding the components related to the artifact.

E. Results of Simulation Study

Fig. 1(a) shows a simulated signal $\mathbf{X}$ with an SNR equal to 0.65. The (normalized) components obtained by applying the BSS-CCA algorithm on $\mathbf{X}$ are shown in Fig. 2(a). The autocorrelation of the components is shown in Fig. 2(b). The muscle artifact components are well distinguished from the components related to the brain activity. Moreover, the muscle activity is present in the three lowest autocorrelated components in the CCA decomposition. Excluding those components in the reconstruction of the EEG results in the cleaned EEG shown in Fig. 1(b). Notice that all muscle artifact is removed and the alpha activity is preserved. The RRMSE of the BSS-CCA processed data was equal to 0.11.

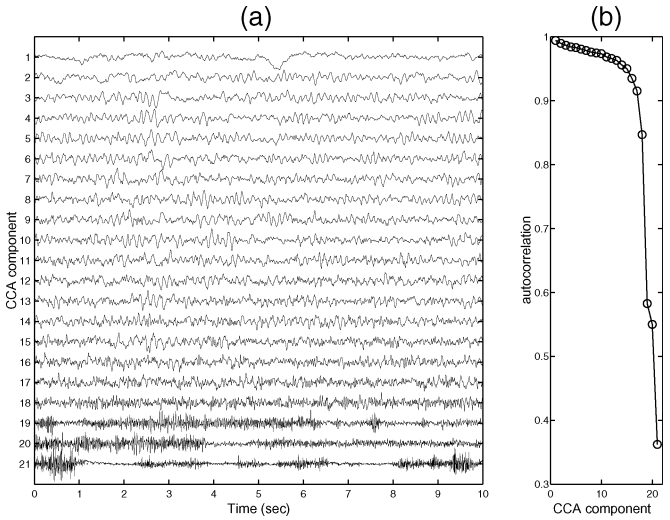

Fig. 2. (a) CCA components (normalized) obtained by applying BSS-CCA on the 10-s EEG epoch shown in Fig. 1(a); (b) The autocorrelation of the CCA components.

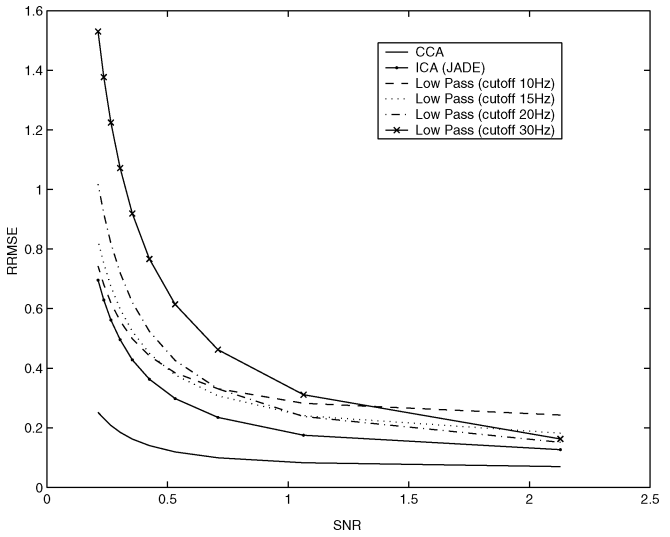

Fig. 3. The RRMSE as a function of SNR on the EEG epoch $\mathbf{B}$ containing alpha (8–13 Hz) activity.

The low-pass filters were not capable of removing all artifact without altering the underlying brain activity because the frequency spectrum of the muscle artifacts overlaps with that of the brain signal in the simulated signal $\mathbf{X}$. The RRMSE of the 10-, 15-, 20-, and 30-Hz low-pass filtered data was equal to 0.35, 0.33, 0.36, and 0.51, respectively.

Also, ICA(JADE) was applied on the simulated signal shown in Fig. 1(a). Since some of the ICA(JADE) components contained both muscle activity and brain activity, the removal of muscle artifact was not complete (since we did not want to remove any brain activity). The RRMSE of the ICA(JADE) processed data was equal to 0.25.

The RRMSE as a function of SNR for the different artifact removal techniques (BSS-CCA, ICA(JADE), and the low-pass filter with cutoff frequency at 10, 15, 20, and 30 Hz) is shown in Fig. 3. SNRs equal to 2.10, 1.07, 0.65, 0.53, 0.42, 0.35, 0.30, 0.26, 0.23, and 0.21 are used. The BSS-CCA method outperformed all methods for all SNRs. The overall RRMSE for BSS-CCA was on average 2.48 ± 0.31 times lower than that of ICA(JADE) and, respectively, 3.15 ± 0.19; 3.12 ± 0.21; 3.55 ± 0.60; 5.07 ± 1.20 times lower than that of the low-pass filter with cutoff equal to 10, 15, 20, and 30 Hz.

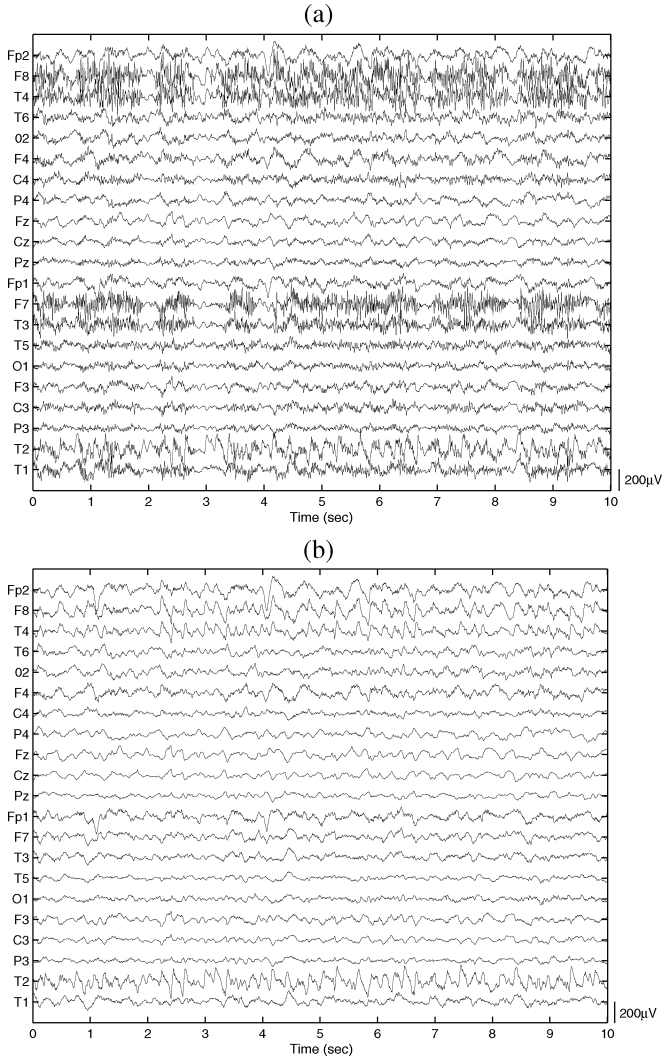

Fig. 4. (a) Original ictal EEG epoch of 10 s; (b) EEG reconstruction after excluding artifactual CCA components. Notice that the muscle artifact was removed completely, while preserving the sharp ictal activity in the right temporal lobe ($T2(=$ right sphenoidal electrode$)$, $F8$, and $T4$).

IV. Method Applied to Ictal EEG Recordings

A. Materials

Ictal EEG is often severely contaminated with muscle artifact, complicating the determination and localization of the ictal onset. Fig. 4(a). shows a 10 s epoch of a scalp EEG recording from a long-term Epilepsy Monitoring Unit. The acquisition settings were the same as for the brain activity in Section III-A. This EEG contains ictal activity from a patient with Mesial Temporal Lobe Epilepsy. The seizure EEG is contaminated with muscle artifact and eye blinks.

B. Results

Again BSS-CCA was applied on the ictal EEG recording shown in Fig. 4(a). We observed that the muscle artifact components were well distinguished from the components related to the brain activity. Moreover, muscle activity was only present in the 10 lowest components

in the CCA decomposition. Excluding those components in the reconstruction of the EEG results in the cleaned EEG shown in Fig. 4(b). Notice that the muscle artifact was removed completely, while preserving the ictal activity on the $T2$, $F8$, and $T4$ electrodes. The ictal activity, which was masked by muscle artifact activity, becomes visible in the BSS-CCA processed recording. Error measures could not be used as we did not have a-priori information available of the brain (epileptic) sources.

V. Discussion

In this paper, a new method for muscle artifact removal in scalp EEG based on CCA was presented. The performance of the method was tested on synthetic data. The method outperformed a low-pass filter with different cutoff frequencies and an ICA(JADE)-based technique for muscle artifact removal.

In addition, the performance of the method was illustrated on a real ictal EEG recording. The muscle artifact was successfully removed without altering the ictal EEG. Both in the synthetic data and in the ictal EEG recording, the muscle activity is well separated from the brain activity in the CCA decomposition. Furthermore, the muscle activity is present in the lowest autocorrelated CCA components, which indicates that they are a more noise like signal (small autocorrelation) compared to the brain activity.

Currently, the BSS-CCA method is being evaluated on 40 ictal EEGs of patients with refractory partial epilepsy and an ictal onset zone that was well-defined during a presurgical evaluation. The preliminary results illustrate that the method improved the interpretation of ictal EEG in a clinically significant way in around 40% of the EEGs compared to low-pass filtering [14]. Moreover, our method never degraded the ictal EEG, illustrating the good separation between ictal EEG and EMG artifact by BSS-CCA in all cases.

Furthermore, the removal of muscle artifact can be used as a preprocessing step to facilitate further signal processing of scalp EEG signals. In this paper, however, the removal of muscle artifact was based on visual inspection of the components. Further research will indicate whether thresholding on the autocorrelation index will be sufficient to remove muscle artifact automatically in a large subject group.

The comparison with temporal decorrelation-based ICA techniques (TDSEP [15], ac-dc [16], SOBI [11], etc.) and the mathematical relationship between CCA and these techniques will be the subject of further research.

Acknowledgment

The authors would like to thank G. Van Driel for his assistance in the preparation of the data.

References

[1] S. Spencer, P. Williamson, S. Bridgers, R. Mattson, D. Cicchetti, and D. Spencer, "eliability and accuracy of localization by scalp ictal EEG," *Neurology*, vol. 30, pp. 1567–1575, 1985.

[2] I. Goncharova, D. McFarland, T. Vaughan, and J. Wolpaw, "EMG contamination of EEG: spectral and topographical characteristics," *Clin. Neurophysiol.*, vol. 114, pp. 1580–1593, 2003.

[3] H. Nam, T.-G. Yim, S. Han, J.-B. Oh, and S. Lee, "Independent component analysis of ictal EEG in medial temporal lobe epilepsy," *Epilepsia*, vol. 43, no. 2, pp. 160–164, 2002.

[4] E. Urrestarazu, J. Iriarte, M. Alegre, M. Valencia, C. Viteri, and J. Artieda, "Independent component analysis removing artifacts in ictal recordings," *Epilepsia*, vol. 45, no. 9, pp. 1071–1078, 2004.

[5] H. Hotelling, "Relations between two sets of variates," *Biometrika*, vol. 28, pp. 321–377, 1936.

[6] O. Friman, M. Borga, P. Lundberg, and H. Knutsson, "Exploratory fMRI analysis by autocorrelation maximization," *NeuroImage*, vol. 16, no. 2, pp. 454–464, 2002.

[7] M. Borga and H. Knutsson, A Canonical Correlation Approach to Blind Source Separation Dept. Biomedical Engineering, Linköping University, Linköping, Sweden, Tech. Rep. LiU-IMT-EX-0062, 2001.

[8] O. Friman, J. Cedefamn, P. Lundberg, M. Borga, and H. Knutsson, "Detection of neural activity in functional MRI using canonical correlation analysis," *Magn. Reson. Med.*, vol. 45, pp. 323–330, 2001.

[9] O. Friman, "Adaptive Analysis of Functional MRI Data," Ph.D. thesis, Dept. Biomed. Eng., Linköpings universitet, Linköping, Linköping, Sweden, 2003.

[10] M. Nuwer, G. Comi, and R. Emmerson *et al.*, "IFCN standards for digital recording of clinical EEG," *Electroencephalogr. Clin. Neurophysiol.*, vol. 106, pp. 259–261, 1998.

[11] A. Belouchrani, K. Abed-Meraim, J.-F. Cardoso, and E. Moulines, "A blind source separation technique using second order statistics," *IEEE Trans. Signal Process.*, vol. 45, no. 2, pp. 434–444, Feb. 1997.

[12] J.-F. Cardoso, "Higher-order contrast for independent component analysis," *Neural Comput.*, vol. 11, pp. 157–192, 1999.

[13] J. Iriarte, E. Urrestarazu, M. Valencia, M. Alegre, A. Malanda, C. Viteri, and J. Artieda, "Independent component analysis as a tool to eliminate artifacts in EEG: a quantitative study," *J. Clin. Neurophysiol.*, vol. 20, no. 4, pp. 249–257, 2003.

[14] W. De Clercq, A. Vergult, B. Vanrumste, S. Van Huffel, M. Kokarakis, J. V. Hees, A. Palmini, and W. Van Paesschen, "Improving the interpretation of the ictal scalp electroencephalogram: a new muscle artifact removal technique," *Epilepsia*, vol. 46, no. 6 (suppl.), p. 378, 2005.

[15] A. Ziehe and K. Mller, "TDSEP—an efficient algorithm for blind separation using time structure," in *Proc. 8th Int. Conf. Artificial Neural Networks, ICANN'98, Perspectives in Neural Computing*, 1998, pp. 675–680.

[16] A. Yeredor, "Non-orthogonal joint diagonalization in the least-squares sense with application in blind source separation," *IEEE Trans. Signal Process.*, vol. 50, no. 7, pp. 1545–1553, Jul. 2002.